Research Article | Vol. 26, No. 9 | 30 Apr 2018 | OPTICS EXPRESS 12038

Optics EXPRESS

Fine tuning method for optimization of liquid crystal based polarimeters

ALBERTO ÁLVAREZ-HERRERO,* PILAR GARCÍA PAREJO, AND MANUEL SILVA-LÓPEZ

Instituto Nacional de Técnica Aeroespacial (INTA), Área de Óptica Espacial, Carretera de Ajalvir, Km. 4, Torrejón de Ardoz, 28850 Madrid, Spain
alvareza@inta.es

Abstract: Liquid crystal variable retarders (LCVR) based polarimeters perform temporal polarization modulation by applying a sequence of driving voltages to introduce different optical retardances. However, even after a careful design and fabrication, manufacturing tolerances (i.e., slight optical axis misalignments, instrument residual polarization, optical activity in the LCVRs...) or the final system configuration (i.e., LCVRs in a convergent optical beam, thermal gradient across the clear aperture...) produce deviations from the ideal setup. As a consequence, all of these effects can reduce the polarimetric modulation efficiency of the device and, therefore, its signal-to-noise ratio. Hence, the voltage sequence applied according to the LCVR calibration curves may not be suitable to reach the optimal theoretical polarimetric efficiencies. In this work, a systematic fine tuning method for the LCVRs driving voltages is described an experimentally demonstrated.

© 2018 Optical Society of America under the terms of the OSA Open Access Publishing Agreement

OCIS codes: (230.3720) Liquid-crystal devices; (120.5410) Polarimetry; (110.5405) Polarimetric imaging; (350.6090) Space optics.

References and links

1. A. Álvarez-Herrero, N. Uribe-Patarroyo, P. García-Parejo, J. Vargas, R. L. Heredero, R. Restrepo, V. Martínez-Pillet, J. C. del Toro Iniesta, A. López, S. Fineschi, G. Capobianco, M. Georges, M. López, G. Boer and I. Manolis, "Imaging polarimeters based on Liquid Crystal Variable Retarders: an emergent technology for space instrumentation," Proc. SPIE **8160**, 81600Y (2011).
2. F. Snik, J. Craven-Jones, M. Escuti, S. Fineschi, D. Harrington, A. De Martino, D. Mawet, J. Riedi and J. S. Tyo, "An overview of polarimetric sensing techniques and technology with applications to different research fields," Proc. SPIE **9099**, 90990B (2014).
3. J. C. del Toro Iniesta and M. Collados, "Optimum modulation and demodulation matrices for solar polarimetry," Appl. Opt. **39**(10), 1637–1642 (2000).
4. J. S. Tyo, "Design of optimal polarimeters: maximization of signal-to-noise ratio and minimization of systematic error," Appl. Opt. **41**(4), 619–630 (2002).
5. V. de Martino, E. García-Caurel, B. Laude and B. Drévillon, "General methods for optimized design and calibration of Mueller polarimeters," Thin Solid Films **455-456**, 112–119 (2004).
6. J. C. del Toro Iniesta and V. Martínez-Pillet, "Assessing the behavior of modern solar magnetographs and spectropolarimeters," The Astrophysical Journal Supplement Series **201**, 22 (2012).
7. A. Álvarez-Herrero, P. García-Parejo, H. Laguna, J. Villanueva, J. Barandiarán, L. Bastide, M. Reina, A. Sanchez, A. Gonzalo, R. Navarro, I. Vera and M. Royo, "Polarization modulators based on Liquid Crystal Variable Retarders for the Solar Orbiter mission," Proc. SPIE **9613**, 96130I (2015).
8. A. Gandorfer, S. K. Solanki, J. Woch, V. Martínez-Pillet, A. Álvarez-Herrero and T. Appourchaux, "The Solar Orbiter Mission and its Polarimetric and Helioseismic Imager," J. Phys. Conf. Ser. **271**, 012086 (2011).
9. N. Uribe-Patarroyo, A. Álvarez-Herrero and V. Martínez-Pillet, "Preflight calibration of the Imaging Magnetograph eXperiment polarization modulation package based on liquid-crystal variable retarders," Appl. Opt. **51**(21), 4954–4970 (2012).

1. Introduction

Polarimeters are increasingly used in applications such as biomedical, remote sensing, earth observation or astrophysics. In this context, the polarization modulators based on Liquid Crystal

#309373 https://doi.org/10.1364/OE.26.012038
Journal © 2018 Received 18 Oct 2017; revised 8 Feb 2018; accepted 12 Feb 2018; published 26 Apr 2018

Optics EXPRESS

Variable Retarders (LCVRs) are a wide-spread technology used in many of these instruments [1,2].

Specifically, LCVRs become a powerful alternative for space applications since they avoid the traditional rotatory polarizing optics, therefore mechanisms, reducing mass and volume. These are significant advantages for an instrument on board a spacecraft where the resources are very limited and the risk of a mechanical failure should be minimized.

It is well-known that an optimized polarization modulation scheme shall be selected [3–5] in order to minimize the uncertainties propagation and to achieve the required signal-to-noise ratio. In the case of a liquid crystal based polarimeter, that means to select the proper values of the optical retardances for the LCVRs and, therefore, their corresponding driving voltages.

Nevertheless, for real systems, deviations from the theoretical configuration should be taken into account [1]. The manufacturing tolerances of the optical elements and the mechanical assembly produce variations from the ideal case. In fact, the azimuth angles between the polarizing elements (LCVRs, polarizer, etc.) will have some differences with respect to the designed values. Also the LCVRs will present manufacturing imperfections as optical activity, due to molecules twisting effects, because of non-perfect parallel alignment layers between both substrates of the LCVR cell. The instrumental residual polarization will also produce deviation from the theoretical performance.

Additionally, the final configuration of a polarization modulator in the instrument will play a role in the optical response. The two typical configurations are the polarization modulator in a collimated beam or close to an image plane. In the first case, light beams with different angles of incidence correspond to the specific fields of the Field of View (FoV). They will be subjected to different retardances due to the retarders dependence on the incidence angle. In the second configuration, the cones of light corresponding to different fields going through the LCVRs will produce a depolarization effect (the lower the f-number, the higher the depolarization effect).

Finally, other effects such as a thermal gradient across the clear aperture will modify in the polarization response of the modulator. A passive and active thermal control can be implemented in order to minimize this issue but, in any case, it will produce a deviation from the theoretical ideal system.

Many of the effects described above induce a polarization modulation different from the theoretical one, but it does not produce depolarization of the incoming light. That means that most of these effects can be managed changing slightly the foreseen driving voltages for the LCVRs in order to recover an optimal modulation scheme. That is what is called fine-tuning of the polarization modulator.

In this work, a method to carry out the fine-tuning of a LCVRs based polarization modulator and its application is presented. First, the Polarization State Analyzer (PSA) of the Polarimetric and Helioseismic Imager (PHI) for the Solar Orbiter space mission is described (Section 2). Secondly, the theoretical fundamentals for the fine-tuning procedure are presented in Section 3. Finally, the experimental details as well as the results obtained with the PHI PSA are shown in Sections 4 and 5, respectively.

2. Polarimeters based on LCVRs

2.1. Description

The PSA scheme used for the PHI instrument is a standard in many polarimeters based on LCVRs [5,6], nevertheless this will be the first time that liquid crystals will be used on board a space mission for polarimetric measurements [7]. These devices will be used in the Full Disk Telescope and the High Resolution Telescope of PHI [8]. The PSA consists of two Anti-Parallel Nematic LCVRs oriented with their fast axes at 45° with respect to each other followed by a linear polarizer (the polarization analyzer) at 0° with respect to the fast axis of the first LCVR [Fig. 1]. Note that we will consider the transmission axis of the linear polarizer the origin of the angles reference system for the other polarizing elements and the polarization states.

Optics EXPRESS

Each LCVR cell consists of two glass substrates of 5 mm thickness, coated on one side with Indium Tin Oxide and on the other side with and anti-reflective coating. A detailed description of these LCVRs can be found in [7].

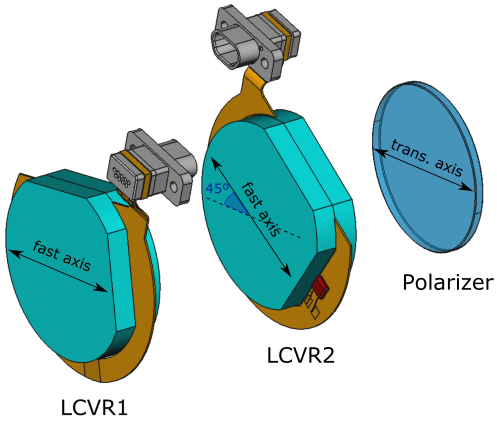


Fig. 1. Scheme of the Polarization State Analyzer of the PHI solar spectro-polarimeter.

The polarization modulator generates four modulations of the polarization state in order to extract the Stokes parameters of the incoming light. Then the polarization state of the incoming light is deduced from the intensity measurements at the detector and the known modulations induced in the polarization. The polarization modulations are known due to the fact that the LCVRs are previously calibrated and the relationship between applied voltage and optical retardance is known. A typical calibration curve of a LCVR is shown in Fig. 2. It corresponds to the LCVR_1 used in the PHI PSA and it was obtained using a Variable Angle Spectroscopic Ellipsometer (VASE) from J. A. Woollam Co. Inc.. The plot illustrates the voltage-retardance dependence at a given temperature. The calibration curves provide the starting point to the fine tuning procedure once the polarimeter is assembled, as it will be explained.

2.2. Modulation matrix and efficiencies

The application of an electric field to the PSA LCVRs produces a specific optical retardance. Hence, the voltages (V_{1i}, V_{2i}) applied to each LCVR will correspond to a couple of retardances associated (ρ_i, σ_i), with $i = 1, 2, 3, 4$.

Mathematically, for each modulation state i, the PSA can be represented by the Mueller matrix of each polarizing element, i.e: the two LCVRs and the polarizer. Taking into account that only the intensity component of the outcoming Stokes vector from the PSA can be measured in the detector, it suffices to construct the so-called modulation matrix $\mathbf{O}$, consisting of each first row of the four PSA Mueller matrices. The inverse of the modulation matrix is the demodulation matrix, $\mathbf{D}$, and it allows to extract the incoming Stokes vector from the intensity measurements in the detector.

It can be shown that the modulation matrix that describes our polarimeter is

$$\mathbf{O} = \begin{pmatrix} 1 & \cos\sigma_1 & \sin\sigma_1 \sin\rho_1 & -\sin\sigma_1 \cos\rho_1 \\ 1 & \cos\sigma_2 & \sin\sigma_2 \sin\rho_2 & -\sin\sigma_2 \cos\rho_2 \\ 1 & \cos\sigma_3 & \sin\sigma_3 \sin\rho_3 & -\sin\sigma_3 \cos\rho_3 \\ 1 & \cos\sigma_4 & \sin\sigma_4 \sin\rho_4 & -\sin\sigma_4 \cos\rho_4 \end{pmatrix},$$

Optics EXPRESS

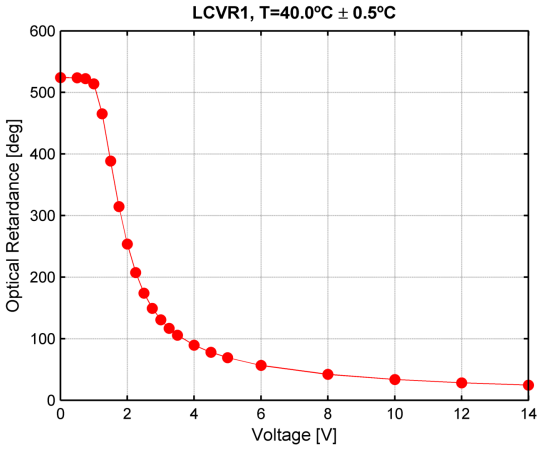


Fig. 2. Volts vs. retardance plot measured at T= 40.0 °C ± 0.5 °C for $LCVR_1$. Past the point of the Fréedericksz transition, the higher the applied voltage, the lower the optical retardance.

where ρ_i and σ_i correspond to the sequence of four optical retardances applied to $LCVR_1$ and $LCVR_2$ respectively. This polarization modulation scheme was selected taking into account that the number of modulation states shall be minimized due to the Solar Orbiter mission constraints (i.e.: total acquisition time), even though the signal-to-noise (SNR) shall be maximized.

Hence the design of a polarimeter relies on obtaining a modulation scheme whose matrices **O** and **D** optimally provide the measured Stokes parameters. Moreover, the polarimetric accuracy is related to the efficiency of the modulation scheme which provides the uncertainty propagation from the intensity measurements to the deduced Stokes parameters and, therefore, the SNR. This efficiency is defined in [3] as:

$$\varepsilon_i = \left(n \sum_{j=1}^{n} D_{ij}^2 \right)^{-1/2} . \tag{1}$$

These four-components form the so-called efficiency vector ε where n is the number of intensity measurements, i.e. modulation states. Then each Stokes parameter, S_i, is determined with a corresponding efficiency given by ε_i. Notice that each row of **D** will set an efficiency vector component.

The efficiency vector components fulfil the following relationship:

$$\varepsilon_1 \leq 1, \quad \sum_{i=2}^{4} \varepsilon_i^2 \leq 1. \tag{2}$$

According to this the maximum theoretical efficiencies, in which we define as a goal equal SNR in all Stokes parameters, are $\varepsilon_1 = 1$ and $\varepsilon_{2,3,4} = \frac{1}{\sqrt{3}}$.

The SNR of the Stokes parameter S_1 is related to the single-shot s/n through

$$(\mathrm{S/N})_1 = (\mathrm{s/n})\varepsilon_1 \sqrt{N_p N_a}, \tag{3}$$

where N_p and N_a are the number of single detector shots and the accumulations number respectively as explained in [6].

Then, the SNR for Stokes $S_{2,3,4}$ can be calculated using the following relationship:

Optics EXPRESS

$$(\mathrm{S/N})_i = \frac{\varepsilon_i}{\varepsilon_1}(\mathrm{S/N})_1. \tag{4}$$

Thus, depending on the retardances of the LCVRs we will obtain a particular **O**. A good selection of these retardances will optimize the SNR. An optimum modulation scheme that maximizes the polarimetric efficiencies is the one selected for PHI and shown in Table 1. Notice that the LCVR_1 presents the same retardance in modulation 1 and 2, and in modulation 3 and 4.

Table 1. Retardance chart selected. It is an optimum modulation scheme in ideal PSA.

Modulation	**LCVR_1 [deg]**	**LCVR_2 [deg]**
1	ρ_1=225	σ_1=234.74
2	ρ_1=225	σ_2=125.26
3	ρ_2=315	σ_3=54.74
4	ρ_2=315	σ_4=305.26

It can be seen that using this set of retardances produces a modulation matrix, where the second, third and fourth column have values of $\pm\frac{1}{\sqrt{3}}$ ($\approx \pm 0.577$):

$$\mathbf{O}_{opt} = \begin{pmatrix} 1 & \frac{-1}{\sqrt{3}} & \frac{1}{\sqrt{3}} & \frac{-1}{\sqrt{3}} \\ 1 & \frac{-1}{\sqrt{3}} & \frac{-1}{\sqrt{3}} & \frac{1}{\sqrt{3}} \\ 1 & \frac{1}{\sqrt{3}} & \frac{-1}{\sqrt{3}} & \frac{-1}{\sqrt{3}} \\ 1 & \frac{1}{\sqrt{3}} & \frac{1}{\sqrt{3}} & \frac{1}{\sqrt{3}} \end{pmatrix}. \tag{5}$$

This matrix provides the highest theoretical components for the efficiency vector $\varepsilon = (1, 0.577, 0.577, 0.577)$. Note that a well-balanced efficiency vector is the goal for PHI since we are interested in the measurement of the full Stokes vector with identical SNR in each component.

3. Fine tuning method

From Eq. (1) it can be seen that to maximize all the components of the efficiency vector one has to act on each row of **D** separately. However, the relation between the D_{ij} and the ρ and σ elements is not simple. We have chosen to analyze the existence of **D** as a function of **O**, and then illustrate graphically the dependence on the efficiency.

Given the modulation matrix formed by the retardance modulation sequence presented in Table 1

$$\mathbf{O} = \begin{pmatrix} 1 & \cos\sigma_1 & \sin\sigma_1 \sin\rho_1 & -\sin\sigma_1 \cos\rho_1 \\ 1 & \cos\sigma_2 & \sin\sigma_2 \sin\rho_1 & -\sin\sigma_2 \cos\rho_1 \\ 1 & \cos\sigma_3 & \sin\sigma_3 \sin\rho_2 & -\sin\sigma_3 \cos\rho_2 \\ 1 & \cos\sigma_4 & \sin\sigma_4 \sin\rho_2 & -\sin\sigma_4 \cos\rho_2 \end{pmatrix}. \tag{6}$$

Its determinant can be written as:

$$\begin{aligned} det(\mathbf{O}) = {} & [\cos\rho_2 \sin\rho_1 - \cos\rho_1 \sin\rho_2] \times \big[\cos\sigma_1 \sin\sigma_2 (\sin\sigma_3 - \sin\sigma_4) \\ & + \cos\sigma_2 \sin\sigma_1 (\sin\sigma_4 - \sin\sigma_3) + \cos\sigma_3 \sin\sigma_4 (\sin\sigma_2 - \sin\sigma_1) \\ & + \cos\sigma_4 \sin\sigma_3 (\sin\sigma_1 - \sin\sigma_2)\big]. \end{aligned} \tag{7}$$

Then, it can be seen that the modulation matrix is singular when

Optics EXPRESS

$$det(\mathbf{O}) = 0 \begin{cases} \text{if } \sigma_1 = \sigma_2 \\ \text{if } \sigma_3 = \sigma_4 \\ \text{if } \tan\rho_1 = \tan\rho_2 \\ \text{if } \frac{\cos\sigma_2 \sin\sigma_1 - \cos\sigma_1 \sin\sigma_2}{\sin\sigma_2 - \sin\sigma_1} = \frac{\cos\sigma_3 \sin\sigma_4 - \cos\sigma_4 \sin\sigma_3}{\sin\sigma_4 - \sin\sigma_3} \end{cases} . \quad (8)$$

The first two conditions are trivial, since we are making two rows of the modulation matrix identical. The third and fourth condition can be deduced algebraically by making the two main factors of $det(\mathbf{O})$ equal to 0. In these conditions, $\mathbf{O}$ is not invertible and $\mathbf{D}$ does not exists. As a consequence, there is no efficiency vector if $\mathbf{O}$ meets any of these conditions.

Figure 3 shows the efficiency vector components plotted as a function of one retardance at a time. In particular Fig. 3(a) shows the ε_i components as a function of σ_1, chosen as variable. The rest of the retardances are as in Table 1.

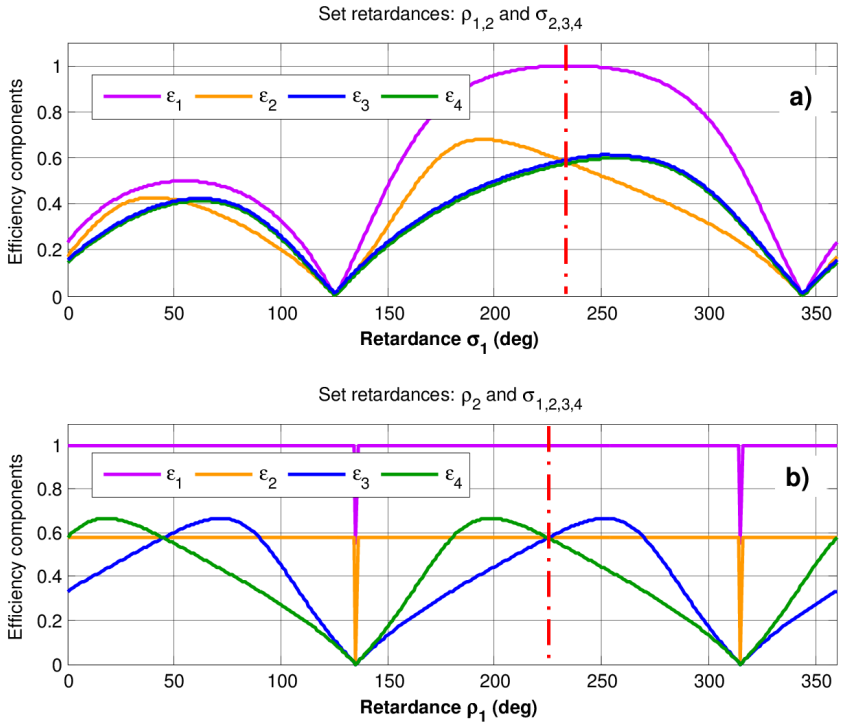


Fig. 3. Efficiency vector components plotted against one retardance chosen as variable. a) All the efficiency vector components are dependent on the first retardance applied to the $LCVR_2$. b) Two efficiency components are constant under changes in the first retardance of the $LCVR_1$. The vertical dashed line shows the actual retardances applied according to Table 1.

It can be seen that the ε_i components are all dependent on this retardance since $LCVR_2$ is placed at 45 ° with respect to the analyzer and, therefore, all the Stokes vector components are modified. Similar curves can be obtained with any σ_i as variable. The zeros observed at $\sigma_1 = 125.26°$ and 344.20° are actually situations where $det(\mathbf{O}) = 0$. Overall the efficiency drops as the matrix rows are less independent, and the condition number of $\mathbf{O}$ increases (becames ill-conditioned). Alternatively, the red vertical line marks the best compromise, where the efficiencies ε_2, ε_3 and ε_4

Optics EXPRESS

have the same value and the inequalities from Eq. (2) are maximized. In this case, the retardances correspond to the ones shown in Table 1.

On the other hand, Fig. 3(b) shows the calculated efficiency components as a function of ρ_1. Using this retardance as variable leaves two efficiency components constant. In particular ε_1 and ε_2 are not dependent on ρ_1. Similar curves can also be obtained using ρ_2 as variable. This means that one can act on the $LCVR_2$ retardance to improve $\varepsilon_{3,4}$ without altering the others. It can be intuitively understood due to the fact that the $LCVR_1$ is parallel to the analyzer. Therefore it does not produce any modulation to the second component of the Stokes vector, the one that corresponds to the horizontal-vertical lineal polarization. Consequently, changes in its retardance have no effect on ε_2.

The zeros in Fig. 3(b) at $\rho_1 = 135°$ and 315° correspond again to situations where **D** does not exists (**O** is singular). The red line also marks the best compromise achievable using the values shown in Table 1. Around this optimum situation it can be seen that increasing ε_3 implies reducing ε_4 and viceversa.

Summarizing, Fig. 3 shows that the first two rows of the demodulation matrix **D** depend only on σ_i. This means that the first two components of the efficiency vector can be maximized by just tuning the $LCVR_2$ voltages. On the contrary, the third and fourth row of **D** depend on both ρ_i and σ_i. This is an important result that provides us with a road map for an optimization procedure.

Keeping this in mind, it is convenient to focus on the modulation matrix experimentally obtained and compare it to the ideal one $\mathbf{O}_{opt}$. The fundamental idea of the procedure is to sequentially modify ρ_i and σ_i to achieve the values of the ideal modulation matrix [Eq. (5)]. The method is followed, regardless particular efficiencies values obtained during the intermediate steps, until we reach a modulation matrix close enough to the ideal one. A scheme of the method is shown in Fig. 4.

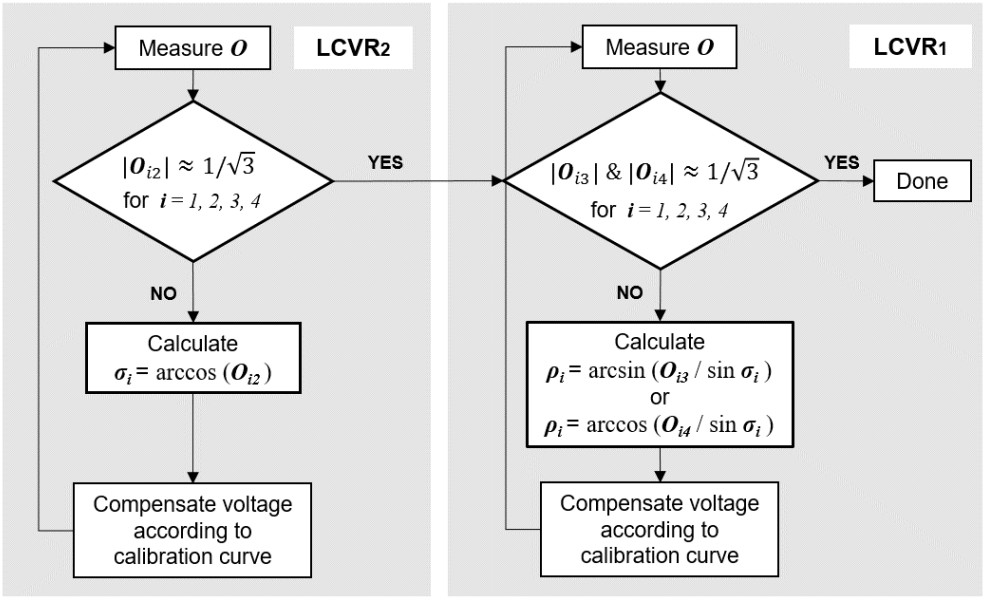


Fig. 4. Step by step procedure of the fine-tuning method.

Therefore, the best way to modify a given modulation matrix is to start by changing σ_i to make the second column of **O** more similar to $\mathbf{O}_{opt}$ [Eq. (5)]. This means fine tuning the voltages provided to the $LCVR_2$ in the first place. To do that is to calculate the *arccos* of the matrix

Optics EXPRESS

components $O_{i,2}$. This provides the retardance that it is actually applied and its deviation from the ideal value. Then, and according to its voltage-retardance calibration curve, this offset is compensated varying the voltage conveniently. Note that the use of the LCVR calibration curve is necessary because of the non-linear dependence of the retardance with the applied voltage. This process for each σ_i sets the optimum values for ε_1 and ε_2. However, this will also modify the other matrix components, and can make worse the other efficiency components. Then we proceed to the next step.

Once the σ_i are set, the process follows by tuning the voltages of $LCVR_1$. By tuning the voltages associated to ρ_i following the same method and taking into account that σ_i is known from second column of $\mathbf{O}$. Then the actual ρ_i and its deviation can be deduced calculating the $arcsin$ from the third column or alternatively the $arccos$ from the fourth column.

The right half of the modulation matrix $\mathbf{O}$ is then changed and their components become more similar, improving $\varepsilon_{3,4}$ in the process. Theoretically they will have no impact on $\varepsilon_{1,2}$, so that the whole vector can be optimized. In practice we do expect some cross-coupling effects among the matrix components and therefore among the efficiency vector components. This can be due to experimental issues such as uncertainty on instrumental measurements as well as effects from the deviation of an ideal PSA. In any case this procedure can be iterated until satisfactory results are obtained.

To evaluate the goodness of the modulation matrix obtained experimentally (O_{step}) we have computed the root mean square error ($RMSE$) as a figure of merit. This is defined as

$$RMSE = \sqrt{\frac{\sum_{i,j}\left[(O_{opt})_{ij} - (O_{step})_{ij}\right]^2}{4 \times n}}, \tag{9}$$

where n is the number of modulation states. This parameter allows us to quantify the improvement within the fine tuning iterative process.

4. Experimental details

The proposed fine tuning method was used in the flight model of the PHI PSA. In order to calibrate it and to carry out the measurement of its polarimetric modulation efficiencies, a Polarization State Generator (PSG) was developed according to the PHI optical configuration. The PSG allows to characterize and calibrate a PSA in a collimated or a telecentric beam. In this work, the results obtained using the first configuration will be discussed, which implies that each analysed pixel (each image field) in the camera corresponds to a beam with an incidence angle in the PSA. The calibration system was analogous to the one described in [9]. It consisted of a fixed polarizer and a rotating quarter-waveplate (QWP) in an imaging projector. This was formed by an achromatic doublet of 200 mm focal length (AC508-200-A-ML from Thorlabs) and a diffused object of 7 mm × 7 mm that provided a collimated beam of ±2 deg of FoV. The polarizer and the QWP were located between the object and the lens and the incidence angles on them were under their acceptance angles in order to guarantee an homogeneous polarization state over the full FoV. The illumination source was the high power LED M617L3 from Thorlabs emitting at $\lambda = 617$ nm. The retardance of the QWP (10RP34-6328 from Newport, zero-order polymer wave-plate), originally designed for $\lambda = 632.8$ nm, was measured at that interest wavelength with a Variable Angle Spectroscopic Ellipsometry (VASE) from J.A Woollam, obtaining a value of 0.2588λ within an acceptance angle of ±10 deg. Finally, an imaging optics and a camera was included in the setup after the PHI PSA. The imaging optics was an achromatic doublet of 150mm focal length (AC508-150-A-ML from Thorlabs) and the camera was a Photonfocus MV1-D2080(IE)-G2. The PHI PSA includes an active thermal control which was set to 40.0 °C ± 0.5 °C.

Optics EXPRESS

5. Results

To demonstrate the process we have performed a complete polarimetric characterization of the PSA using the arrangement described in Section 4. The procedure described in Section 3 is applied to maximize its modulation matrix and efficiency vector.

The purpose of the calibration is to obtain its modulation matrix **O** using a set of known incoming polarization states produced by the PSG. In order to assess and consider possible inhomogeneities in the PHI PSA, the calibration is performed pixel by pixel.

As previously described, the PSA was placed in the optical path of a collimated beam with its clear aperture fully illuminated. Firstly, the PSG was used to generate a reduced set of 19 polarimetric input states. This corresponds to 5° rotations of the QWP along a quarter of the full rotation. This number is enough to obtain a first good estimation of **O** in a reduced time in order to have handle times for the feedback during the fine-tuning process. Nevertheless, the final calibration is carried out using a complete set of 73 polarimetric input states (a full rotation of the QWP) to enhance the accuracy of the **O** determination.

The PHI PSA was modulated following the sequence described in Table 1 and the calibration curves of each individual LCVR. Then the first experimental modulation matrix obtained was (note that it is the mean **O** across the FoV):

$$O_{initial} = \begin{pmatrix} 1.018 & -0.774 & 0.348 & -0.452 \\ 0.972 & -0.290 & -0.494 & 0.853 \\ 0.983 & 0.831 & -0.572 & -0.223 \\ 1.027 & 0.188 & 0.673 & 0.596 \end{pmatrix}, \qquad RMSE = 0.1994,$$

which is clearly very different from Eq. (5) as shown the *RMSE*. The efficiency vector that is computed from this modulation is $\varepsilon = [0.943, 0.550, 0.496, 0.545]$. These are efficiencies not far from maximum theoretical values, however we will show that they can be improved by making $O_{initial}$ more similar to the ideal one.

Thus, as explained in Section 3 the voltages will be fine tuned to optimise this efficiency. First the $\mathbf{O_{i2}}$ column was optimised following Fig. 4 and, therefore, tuning σ_i corresponding to LCVR_2. The modulation matrix obtained in this first step was:

$$O_{step1} = \begin{pmatrix} 1.024 & -0.595 & 0.533 & -0.627 \\ 0.955 & -0.581 & -0.386 & 0.694 \\ 0.991 & 0.518 & -0.739 & -0.338 \\ 1.031 & 0.461 & 0.678 & 0.420 \end{pmatrix}, \qquad RMSE = 0.1137.$$

As result the terms $\mathbf{O_{12}}$ and $\mathbf{O_{22}}$ are closer to ideal ones (green terms) and a lower value of *RMSE* was obtained. Nevertheless $\mathbf{O_{32}}$ and $\mathbf{O_{32}}$ need another iteration (orange terms). It is carried out in the step 2, together with the tuning of the $\mathbf{O_{13}}$, $\mathbf{O_{14}}$, $\mathbf{O_{23}}$ and $\mathbf{O_{24}}$ elements corresponding to ρ_1 for LCVR_1. Then, the following result was measured:

$$O_{step2} = \begin{pmatrix} 1.022 & -0.585 & 0.569 & -0.538 \\ 0.960 & -0.551 & -0.427 & 0.644 \\ 0.989 & 0.553 & -0.679 & -0.317 \\ 1.029 & 0.523 & 0.627 & 0.357 \end{pmatrix}, \qquad RMSE = 0.1043.$$

Later, the tuning of ρ_2 for LCVR_1 was carried out, improving the values of the elements $\mathbf{O_{33}}$, $\mathbf{O_{34}}$, $\mathbf{O_{43}}$ and $\mathbf{O_{44}}$ and decreasing the *RMSE*:

$$O_{step3} = \begin{pmatrix} 1.025 & -0.587 & 0.572 & -0.538 \\ 0.962 & -0.552 & -0.432 & 0.644 \\ 0.986 & 0.547 & -0.649 & -0.387 \\ 1.027 & 0.538 & 0.585 & 0.4091 \end{pmatrix}, \qquad RMSE = 0.0823.$$

Optics EXPRESS

Even though the improvement was evident, the procedure was repeated until achieving a better similarity with respect to the ideal modulation matrix. Finally, a complete set of 73 polarimetric input states was performed to increase the accuracy. Note that the noise reduction is evident in the first column of the obtained final **O**:

$$O_{final} = \begin{pmatrix} 1.002 & -0.573 & 0.640 & -0.471 \\ 0.996 & -0.598 & -0.508 & 0.587 \\ 0.998 & 0.548 & -0.558 & -0.547 \\ 1.004 & 0.589 & 0.518 & 0.515 \end{pmatrix}, \qquad RMSE = 0.0440.$$

This is clearly a more similar matrix to Eq. (5) as the final value of the *RMSE* shows. The efficiency vector obtained is also very close to the ideal one $\varepsilon = [0.997, 0.576, 0.558, 0.531]$. However, note that ε_4 has not been improved. This is due to residual non-compensated effects of the non-ideal components. The initial efficiency was very high, 0.545 (94% of the theoretical maximum). Finally ε_4 was still close to the theoretical maximum (92%) and the complete efficiency vector was improved.

Taking into account Eq. (3) and (4) it can be found that ratio between the initial and the final SNR is the corresponding efficiencies ratio. Then, we find that the changes after the fine tuning process in the SNR Stokes parameters are (5%, 5%, 13%, −3%). Since we started from a very well optimized system with very high efficiency values, the improvement is clear but not very large. Nevertheless, the general validity of the method to increase the SNR and to obtain a specific matrix **O** is demonstrated. The LCVR retardance changes from the initial values applied during the fine tuning process were from some degrees up to 25°. They corresponded to voltage differences from 0.3 mV to 1.5 V approximately depending on the location on the LCVR calibration curve [Fig. 2].

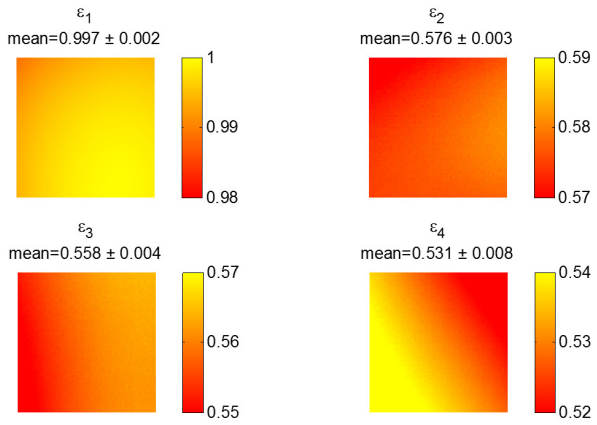


Fig. 5. Polarimetric modulation efficiencies of the PHI PSA for a FoV = ±2 deg.

Figure 5 shows the efficiencies across the full FoV as well as the average efficiencies. Note that the low values of the standard deviation of the mean efficiencies indicates a very low variation across the full FoV. This also can be seen in the plots showing the excellent performance of the PHI PSA after the fine tuning.

Optics EXPRESS

6. Conclusions

A procedure to optimize the polarimetric efficiencies of an LCVR based polarimeter has been demonstrated. Fine tuning the voltages of the LCVRs maximises the efficiency vector components sequentially. This method has been tested and demonstrated with a Polarization State Analyzer which is part of an instrument to be on board a space mission. The Polarimetric and Helioseismic Imager (PHI) and the Multi Element Telescope for Imaging and Spectroscopy (METIS) for the Solar Orbiter mission, led by the European Space Agency, will be the first space telescopes using liquid crystals variable retarders as polarization modulators. In particular, the fine tuning method presented in this work allowed to achieve values close to the theoretical maximum of the polarimetric efficiencies for PHI during the on ground calibrations improving the SNR of the Stokes parameters up to 13%.

Funding

Ministerio de Economía, Industria y Competitividad (MINECO) (ESP2014-56169-C6-3-R, ESP2016-77548-C5-4-R).

Acknowledgments

The authors are very grateful to all the members of the SO/PHI INTA team. This work would not have been possible without them.

130.206.92.100 {ts '2018-04-27 02:48:50'}